Strong frustration due to competing ferromagnetic and antiferromagnetic interactions: magnetic properties of $M(VO)_2(PO_4)_2$ (M = Ca and Sr)

R. Nath,[1,*] A. A. Tsirlin,[1,2,†] E. E. Kaul,[1,‡] M. Baenitz,[1] N. Büttgen,[3] C. Geibel,[1] and H. Rosner[1]

[1]*Max-Planck-Institut für Chemische Physik fester Stoffe, Nöthnitzer Str. 40, 01187 Dresden, Germany*
[2]*Department of Chemistry, Moscow State University, 119992 Moscow, Russia*
[3]*Experimentalphysik V, Elektronische Korrelationen und Magnetismus, University of Augsburg, D-86135 Augsburg, Germany*

We present a detailed investigation of the magnetic properties of complex vanadium phosphates $M(VO)_2(PO_4)_2$ (M = Ca and Sr) by means of magnetization, specific heat, ^{31}P NMR measurements, and band structure calculations. Experimental data evidence the presence of ferromagnetic and antiferromagnetic interactions in $M(VO)_2(PO_4)_2$, resulting in a nearly vanishing Curie-Weiss temperature $\theta_{\mathrm{CW}} \leq 1$ K that contrasts with the maximum of magnetic susceptibility at 3 K. Specific heat and NMR measurements also reveal weak exchange couplings with the thermodynamic energy scale $J_c = 10 - 15$ K. Additionally, the reduced maximum of the magnetic specific heat indicates strong frustration of the spin system. Band structure calculations show that the spin systems of the $M(VO)_2(PO_4)_2$ compounds are essentially three-dimensional with the frustration caused by competing ferromagnetic and antiferromagnetic interactions. Both calcium and strontium compounds undergo antiferromagnetic long-range ordering at $T_N = 1.5$ K and 1.9 K, respectively. The spin model reveals an unusual example of controllable frustration in three-dimensional magnetic systems.

PACS numbers: 75.50.Ee, 75.40.Cx, 71.20.Ps, 75.30.Et

I. INTRODUCTION

Low-dimensional and/or frustrated spin systems are a subject of thorough studies due to their variety of unusual ground states and quantum phenomena.[1,2] One of the most striking effects in these systems is the formation of a spin-liquid, a dynamically disordered ground state with short-range magnetic correlations. Spin liquids are caused by quantum fluctuations that impede or even suppress long-range magnetic ordering

Quantum fluctuations are enhanced in systems with low spin value, low dimensionality, and/or magnetic frustration. At present, numerous spin models (and the respective structural types) for the frustrated spin systems are known.[3,4] Most of these systems are geometrically frustrated magnets, since the frustration is caused by the topology of the lattice. However, several models reveal frustration due to a specific topology of magnetic interactions, while the lattice itself does not prevent the system from long-range spin ordering. An important advantage of the latter systems is the possibility to vary the degree of frustration by tuning individual exchange couplings. Hence, the formation of different ground states within one model and the access to quantum critical points are possible. Below, we focus on the respective models and briefly review both one-dimensional (1D) and two-dimensional (2D) cases.

The simplest 1D lattice is a uniform chain. To frustrate such a system, one should introduce next-nearest-neighbor (NNN) interaction J_2. Typically, J_2 is antiferromagnetic and competes with either ferromagnetic (FM) or antiferromagnetic (AFM) nearest-neighbor (NN) interactions J_1. The resulting physics strongly depends on the sign of J_1. Thus, for $J_1 > 0$ (i.e., for AFM NN coupling) the system has a dimerized ground state for $J_2/J_1 > 0.241$ that may be further stabilized by lattice distortion as experimentally observed in the spin-Peierls compound $CuGeO_3$.[5,6] If $J_1 < 0$, helical magnetic ordering is formed for $J_2/J_1 < -0.25$, and the pitch angle of the spiral depends on the J_2/J_1 ratio. Recently, a number of frustrated chain systems with $J_2/J_1 < 0$ have been studied,[7] and even the vicinity of the quantum critical point at $J_2/J_1 = -0.25$ was accessed experimentally.[8] In these systems, the possibility to tune the pitch angle by varying the exchange couplings may be particularly attractive due to another intriguing property – the magnetoelectric effect observed in $LiCu_2O_2$ and $LiCuVO_4$.[2,9,10,11,12]

In two dimensions, we will consider the square lattice. Frustration can be introduced by diagonal NNN interactions (J_2) that compete with NN interactions J_1 running along the side of the square. The resulting model is known as a frustrated square lattice (FSL) or $J_1 - J_2$ model. The phase diagram of the FSL has been extensively studied theoretically (see, e.g., Refs. 13,14,15,16). It shows three ordered phases (ferromagnet, Néel antiferromagnet, and columnar antiferromagnet) as well as two critical regions near the quantum critical points at $J_2/J_1 = \pm 0.5$. Basically, these regions are supposed to reveal spin-liquid ground states, although there is also a proposition of a nematic order at $J_2/J_1 = -0.5$.[17] Yet both the conjectures are not verified experimentally, since most of the FSL systems studied so far show columnar magnetic ordering and do not fall to the critical regions. Nevertheless, the detailed investigation of the respective compounds was highly helpful and disclosed important methodological aspects of studying the frustrated spin systems and understanding their physics.[18,19,20,21]

Based on the above representative examples, one may expect that similar changes of the ground state due to the

alteration of the exchange couplings could be realized in other frustrated models – either in one, two, or even three dimensions. This consideration and the recent investigation of an interesting FSL system, the complex vanadium phosphate $Pb_2VO(PO_4)_2$ (Ref. 22), motivated us to start a systematic research of the related compounds. Below, we present the study of $M(VO)_2(PO_4)_2$ (M = Ca, Sr) – two representatives of the same compound family that reveal three-dimensional (3D) spin systems with the frustration caused by the specific topology and magnitudes of the exchange interactions. In the following, we show clear evidence of the frustration in the results of several experimental techniques: magnetization, specific heat, and nuclear magnetic resonance (NMR) measurements. In order to understand the microscopic origin of the frustration, we use band structure calculations.

The outline of the paper is as follows. In Sec. II, we analyze the crystal structure of the $M(VO)_2(PO_4)_2$ compounds focusing on possible paths of the exchange interactions. Methodological aspects are reviewed in Sec. III. Section IV presents experimental results including magnetization, specific heat, and ^{31}P NMR. In Sec. V, we report the results of band structure calculations and construct a microscopic model of the exchange interactions in $Ca(VO)_2(PO_4)_2$. Experimental and theoretical results are compared and discussed in Sec. VI followed by our conclusions.

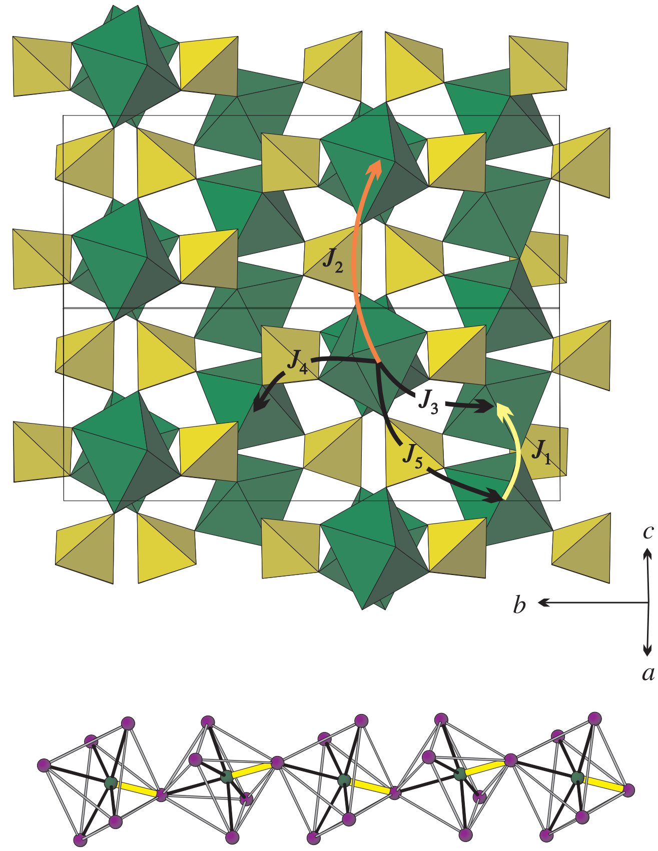

FIG. 1: (Color online) Projection of the $Ca(VO)_2(PO_4)_2$ crystal structure along the [101] direction (upper panel) and the chain of corner-sharing VO_6 octahedra (bottom panel). In the upper panel, the arrows denote different paths of superexchange interactions running via PO_4 tetrahedra. To simplify the figure, calcium atoms are not shown. In the bottom panel, thick (yellow) lines indicate short V–O bonds that are aligned along the direction of the chain.

II. CRYSTAL STRUCTURE

Complex vanadium phosphates $Ca(VO)_2(PO_4)_2$ (Ref. 23) and $Sr(VO)_2(PO_4)_2$ (Ref. 24) are isostructural and crystallize in a face-centered orthorhombic unit cell (space group $Fdd2$, $Z = 8$). The structure presents one vanadium site that shows distorted octahedral coordination. The $V^{+4}O_6$ octahedra share corners to form chains running along the [101] and [$10\bar{1}$] directions. The chains are joined into a 3D-framework by PO_4 tetrahedra (Fig. 1).

Magnetic interactions in insulating transition-metal compounds mainly depend on two factors: the orbital state of the magnetic cation and the possible paths for superexchange interactions. In the following, we will discuss both of these factors.

The orbital state of the magnetic cation is determined by the local environment. In the $M(VO)_2(PO_4)_2$ compounds, vanadium has distorted octahedral coordination with one short bond (see bottom part of Fig. 1). This type of environment is typical for V^{+4} (electronic configuration $3d^1$) and gives rise to a non-degenerate ground state with half-filled d_{xy} orbital (see Refs. 25 and 26 and Sec. V). The d_{xy} orbital is located in the plane perpendicular to the short V–O bond. Short bonds are aligned along the structural chains, therefore the overlap of the half-filled orbital with p orbitals of the two bridging oxygen atoms is very weak, and V–O–V is not an efficient path for superexchange interactions. On the other hand, the d_{xy} orbital may overlap with the p orbitals of four other oxygen atoms providing more complicated V–O–P–O–V paths for the superexchange.

The chains of the VO_6 octahedra in the structures of the $M(VO)_2(PO_4)_2$ compounds are not parallel, and the V–P–O framework looks quite complicated. In order to simplify the situation, one should take into account two considerations: (i) Every vanadium atom is connected to four different PO_4 tetrahedra. (ii) Every PO_4 tetrahedron is connected to four different vanadium atoms. Thus, every vanadium atom may have $3 \times 4 = 12$ different V–O–P–O–V connections at the most. In fact, we find only ten of them, since two connections (namely, that corresponding to J_3) are provided by two tetrahedra simultaneously (see Fig. 1). Some of the connections are equivalent by symmetry and hence give rise to identical exchange interactions. Finally, we find that every vanadium atom can take part in five different superexchange interactions running via PO_4 tetrahedra, and there are two interactions of each type per vanadium atom. We

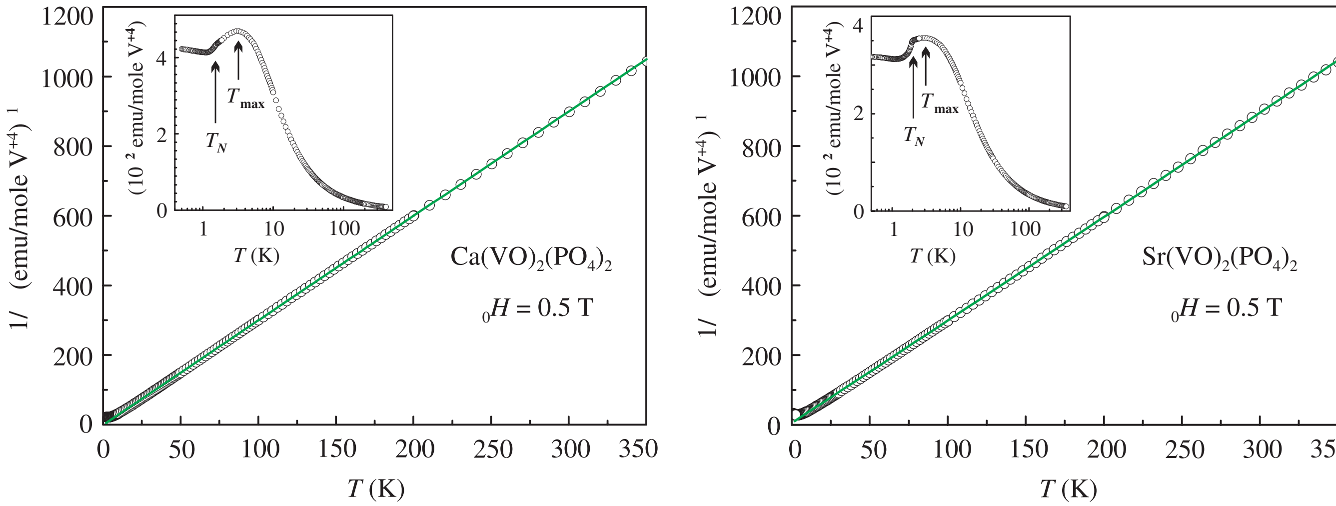

FIG. 2: (Color online) Reciprocal magnetic susceptibility ($1/\chi$) vs. temperature (T) measured at $\mu_0 H = 0.5$ T down to 0.4 K for $Ca(VO)_2(PO_4)_2$ (left panel) and $Sr(VO)_2(PO_4)_2$ (right panel). The solid lines are best fits of the data to Eq. (1). In the insets, χ vs. T is plotted in the logarithmic scale to focus on the $T^{\chi}_{\max}$ and T_N.

denote these interactions and corresponding hoppings by $J_1 - J_5$ and $t_1 - t_5$, respectively (see Fig. 1). J_1 runs along structural chains, J_2 runs between parallel structural chains, while $J_3 - J_5$ provide couplings between non-parallel chains.

According to a recent study of another vanadium phosphate, $Ag_2VOP_2O_7$ (Ref. 25), exchange couplings via PO_4 tetrahedra can hardly be estimated using structural data only. Such couplings depend on numerous geometrical parameters, and slight structural alterations may give rise to a huge change of the exchange integrals. Therefore, we do not attempt to construct a spin model based on qualitative and empirical considerations. Instead, we proceed to the results of band structure calculations and estimate individual exchange couplings (Sec. V). One should be aware that the spin systems of the $M(VO)_2(PO_4)_2$ compounds are intricate and quite complicated even for the computational study due to the weakness of the exchange couplings and the presence of numerous NN and NNN exchange pathways. Therefore, the computational estimates are less accurate as compared to that in other spin-1/2 systems (see, e.g., Refs. 8, 20, and 25). Nevertheless, we succeed to reveal the leading exchange couplings and suggest a plausible scenario of the magnetic frustration in the $M(VO)_2(PO_4)_2$ compounds (see Sec. VI).

III. METHODS

Polycrystalline samples of $M(VO)_2(PO_4)_2$ were prepared by solid state reaction technique using $CaCO_3$ (99.9%), $SrCO_3$ (99.999%), VO_2 (99.99%), and $(NH_4)_2HPO_4$ (99.9%) as starting materials. The synthesis involved two steps. In the first step, the intermediate compounds MP_2O_6 were prepared by firing the stoichiometric mixtures of MCO_3 and $(NH_4)_2HPO_4$ at 850 °C for 1 day in air with one intermediate grinding. In the second step, the intermediate products were mixed with VO_2 in the appropriate molar ratio and heated for 4 days in dynamic vacuum (10^{-5} mbar) with several intermediate grindings and pelletizations. The annealing temperatures were 900 and 850 °C for $Ca(VO)_2(PO_4)_2$ and $Sr(VO)_2(PO_4)_2$, respectively. The resulting samples were single-phase as confirmed by X-ray diffraction (STOE powder diffractometer, CuK_α radiation). Lattice parameters were calculated using a least-squares fit procedure. The obtained lattice parameters for $Ca(VO)_2(PO_4)_2$ [$a = 11.774(2)$ Å, $b = 15.777(3)$ Å, and $c = 7.163(1)$ Å] and $Sr(VO)_2(PO_4)_2$ [$a = 12.008(2)$ Å, $b = 15.924(3)$ Å, and $c = 7.207(1)$ Å] are in agreement with the previously reported values.[23,24]

Magnetization data were measured as a function of temperature and field using a SQUID magnetometer (Quantum Design MPMS). Heat capacity data were collected with Quantum Design PPMS on pressed pellets using the relaxation technique. All the measurements were carried out over a large temperature range (0.4 K $\leq T \leq$ 400 K) in magnetic fields $\mu_0 H$ up to 14 T. The low-temperature measurements were done partly using an additional ^{3}He setup.

The NMR measurements were carried out using pulsed NMR techniques on ^{31}P (nuclear spin $I = 1/2$ and gyromagnetic ratio $\gamma/2\pi = 17.237$ MHz/Tesla) nuclei in a large temperature range (1 K $\leq T \leq$ 300 K). We have done the measurements at a radio frequency of 70 MHz which corresponds to an applied field of about 4.06 T. Low-temperature NMR measurements were partly done using a ^{3}He/^{4}He dilution refrigerator (Oxford Instruments) with the resonant circuit inside the mixing chamber. Spectra were obtained either by Fourier transform (FT) of the NMR echo signals or by sweeping the

field at fixed frequency of 70 MHz. The NMR shift $K(T) = [\nu(T) - \nu_{\rm ref}]/\nu_{\rm ref}$ was determined by measuring the resonance frequency of the sample ($\nu(T)$) with respect to a standard H_3PO_4 solution (resonance frequency $\nu_{\rm ref}$). The ^{31}P spin-lattice relaxation rate ($1/T_1$) was measured by using either a 180° pulse (inversion recovery) or a comb of saturation pulses.

Scalar-relativistic band structure calculations were performed using the full-potential local-orbital scheme (FPLO7.00-27)[27] and the parametrization of Perdew and Wang for the exchange and correlation potential.[28] A k-mesh of 1728 points within the first Brillouin zone (510 in the irreducible part for the space group $Fdd2$) was used. Convergence with respect to the k-mesh was carefully checked.

First, a local density approximation (LDA) calculation was done using the full symmetry of the crystal structure (space group $Fdd2$). The results of this calculation enabled the choice of the orbital states relevant for the magnetic interactions. The respective bands were analyzed using a tight-binding (TB) model, and the resulting hoppings were applied to estimate the antiferromagnetic contributions to the exchange integrals. Such an analysis accounts for all reasonable paths of superexchange and provides a reliable basis for the microscopic model of the magnetic interactions. However, LDA does not give any information about ferromagnetic couplings in the system under investigation.

To account for ferromagnetic interactions in the microscopic model, we performed LSDA+U calculations and compared total energies for four different patterns of spin ordering. Exchange couplings in the $M(VO)_2(PO_4)_2$ compounds are very weak; therefore one has to use the smallest unit cell (i.e., the primitive cell – one-fourth of the face-centered unit cell) in order to achieve the highest possible accuracy. The primitive cell is triclinic (space group $P1$) and includes four inequivalent vanadium atoms, hence a number of different spin configurations can be formed.

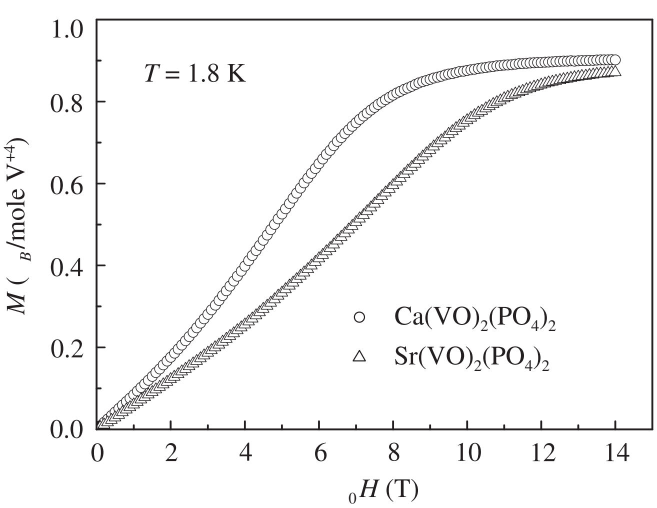

FIG. 3: Isothermal magnetization of the $M(VO)_2(PO_4)_2$ compounds measured at 1.8 K.

Following the results oin Ref. 25, we employed several values of U_d (Coulomb repulsion parameter of the LSDA+U method) in our calculations. According to the previous study,[25] $U_d = 6$ eV provides a reasonable description of the octahedrally coordinated V^{+4} within the FPLO calculations. Yet one should keep in mind that the optimal value of U_d depends on numerous factors (basis set,[29] local environment of the transition-metal cation, and objective parameters), and the unique choice of U_d remains a subtle issue. Below, we use several representative values of U_d (4, 5, and 6 eV) and carefully check their effect on the results. The exchange parameter of LSDA+U was fixed at $J = 1$ eV since usually it has minor importance compared to U_d, especially for the $3d^1$ configuration.

IV. EXPERIMENTAL RESULTS

A. Bulk susceptibility and magnetization

Bulk magnetic susceptibilities (χ) of the $M(VO)_2(PO_4)_2$ compounds are presented in Fig. 2. With decreasing temperature, the susceptibility increases in a Curie-Weiss manner and passes through a broad maximum at $T^{\chi}_{\rm max} \simeq 3$ K. The maximum is characteristic of low-dimensional spin systems and indicates a crossover to a state with antiferromagnetic correlations. The change in slope observed at $T_N = 1.5$ K and 1.9 K [for $Ca(VO)_2(PO_4)_2$ and $Sr(VO)_2(PO_4)_2$, respectively] can be attributed to the onset of long-range magnetic ordering.

To fit the bulk susceptibility data at high temperatures, we use the expression:

$$\chi = \chi_0 + \frac{C}{T + \theta_{\rm CW}} \tag{1}$$

where χ_0 is the temperature-independent contribution that accounts for core diamagnetism and Van Vleck paramagnetism, while the second term is the Curie-Weiss law with the Curie constant $C = N_A\mu^2_{\rm eff}/3k_B$. The data above 20 K were fitted with the parameters listed in Table I. The resulting effective moments $\mu^{\chi}_{\rm eff}$ are in reasonable agreement with the spin-only value of 1.73 μ_B, while the Curie-Weiss temperatures $\theta^{\chi}_{\rm CW}$ for both the compounds are rather small as compared to $T^{\chi}_{\rm max}$ (we use the superscript χ to denote the values related to the analysis of the bulk susceptibility data).

Basically, $T^{\chi}_{\rm max}$ characterizes the energy scale of the magnetic interactions, and $\theta_{\rm CW}$ is a linear combination of all the exchange integrals.[30] Therefore, the reduction in $\theta_{\rm CW}$ as compared to $T^{\chi}_{\rm max}$ implies the presence of both FM and AFM interactions in the system under investigation. Moreover, T_N is considerably lower than $T^{\chi}_{\rm max}$, and this effect may be caused by either low dimensionality and/or frustration of the spin system. As we will show

TABLE I: The parameters of the Curie-Weiss fit [Eq. (1)] of the bulk susceptibility and the NMR shift data (marked by the superscripts χ and K, respectively). χ_0 is the temperature-independent contribution, $\mu_{\rm eff}$ is the effective magnetic moment, and $\theta_{\rm CW}$ is the Curie-Weiss temperature. The listed standard deviations originate from the least-squares fitting.

Sample	χ_0 (10^{-6} emu/mole)	$\mu_{\rm eff}^{\chi}$ (μ_B)	$\theta_{\rm CW}^{\chi}$ (K)	$\mu_{\rm eff}^{K}$ (μ_B)	$\theta_{\rm CW}^{K}$ (K)
$Ca(VO)_2(PO_4)_2$	2.1(5)	1.630(1)	−0.4(3)	1.71(6)	−0.3(1)
$Sr(VO)_2(PO_4)_2$	−1.5(5)	1.653(1)	1.0(1)	1.70(5)	−0.4(1)

below (Sec. V), the spin systems of the $M(VO)_2(PO_4)_2$ compounds are three-dimensional. Thus, the reduction in T_N as compared to $T_{\rm max}^{\chi}$ indicates magnetic frustration in $M(VO)_2(PO_4)_2$.

Field-dependent magnetization data for the $M(VO)_2(PO_4)_2$ compounds are shown in Fig. 3. At low fields, the curves reveal linear behavior, while a positive curvature is observed at higher fields. Further increase in the field results in the saturation at $\mu_0 H_s \simeq 8$ T and 11.5 T for $Ca(VO)_2(PO_4)_2$ and $Sr(VO)_2(PO_4)_2$, respectively. The saturation magnetization (M_s) is about 0.9 μ_B/mole, i.e., slightly below the expected value of 1 μ_B. The underestimate of M_s may be caused by non-magnetic impurities in the samples under investigation. This explanation is further supported by the slight reduction in $\mu_{\rm eff}$ and the magnetic entropy (see Sec. IV B).

The saturation field shows the energy difference between the ground state and the fully polarized (ferromagnetic) state of the system. Thus, the values of H_s can be used to estimate exchange couplings, if the ground state of the system and the leading exchange interactions are known. We will further discuss this point in Sec. VI and employ the H_s values to get quantitative information about exchange couplings in the systems under investigation.

B. Specific heat

The specific heat (C_p) results at zero field are shown in Fig. 4. At high temperatures, C_p is completely dominated by the contribution of phonon excitations; therefore, both the compounds reveal similar $C_p(T)$ curves. With decreasing temperature, C_p starts to increase below $12-15$ K indicating that the magnetic part of the specific heat ($C_{\rm mag}$) becomes prominent. With a further decrease in temperature, $C_p(T)$ shows a broad maximum at around 3 K and 4 K due to the correlated spin excitations and a sharp peak at $T_N = 1.5$ K and 1.9 K associated with the long-range magnetic ordering [the values are given for $Ca(VO)_2(PO_4)_2$ and $Sr(VO)_2(PO_4)_2$, respectively].[31]

In order to get a quantitative estimate of $C_{\rm mag}$, the phonon part $C_{\rm phon}$ was subtracted from the total measured specific heat C_p. The general procedure is similar to that reported in Refs. 32 and 33. The phonon part was estimated by fitting $C_p(T)$ at high temperatures ($15\text{ K} \leq T \leq 200$ K) with a sum of Debye contributions. The additional term A/T^2 accounted for the magnetic contribution, and the final fit was performed using the equation:

$$C_p(T) = \frac{A}{T^2} + 9R\sum_{n=1}^{n=4} c_n \left(\frac{T}{\theta_D^{(n)}}\right)^3 \int_0^{\theta_D^{(n)}/T} \frac{x^4 e^x}{(e^x-1)^2} dx \tag{2}$$

where $R = 8.314$ J/mole K is the gas constant, $\theta_D^{(n)}$ are the characteristic Debye temperatures, and c_n are integer coefficients indicating the contributions of different atoms (or groups of atoms) to the specific heat. The phonon contribution was extrapolated down to 0.4 K and subtracted from the measured $C_p(T)$. The reliability of the whole procedure was justified by integrating $C_{\rm mag}/T$. The resulting magnetic entropies are 5.30 and 5.58 J/mole K [for $Ca(VO)_2(PO_4)_2$ and $Sr(VO)_2(PO_4)_2$, respectively] consistent with the expected value of $R\ln 2$.

High-temperature magnetic contribution A/T^2 is the lowest-order term in the high-temperature series expansion for the specific heat. According to Ref. 30,

$$A = \frac{3R}{32}\sum_i z_i J_i^2 \tag{3}$$

where integers z_i indicate the number of interactions J_i for a single magnetic atom (i.e., coordination number for the interactions of type J_i). The structures of $M(VO)_2(PO_4)_2$ yield $z_i = 2$ for any i (see Sec. II), and we find $A = (3R/16)J_c^2$ with the thermodynamic energy scale of the exchange couplings defined as $J_c = \sqrt{\sum_i J_i^2}$. Using the experimental values $A = 142$ and 147 J K/mole, we estimate $J_c^C = 9.6$ K and 9.8 K for the calcium and strontium compounds, respectively (the superscript C denotes the values obtained from the analysis of the specific heat data).

To interpret the specific heat data, we compare $C_{\rm mag}$ with the simulated curves for the representative spin-1/2 models in both one dimension (uniform chain) and two dimensions (non-frustrated square lattice, triangular lattice), see Fig. 5. The maximum value of the magnetic specific heat ($C_{\rm mag}^{\rm max}$) and the shape of the maximum are characteristic of the magnitude of quantum fluctuations. The enhancement of quantum fluctuations suppresses correlated spin excitations, therefore $C_{\rm mag}^{\rm max}$ is reduced, and the maximum gets broader. One may follow this effect in Fig. 5. The non-frustrated square

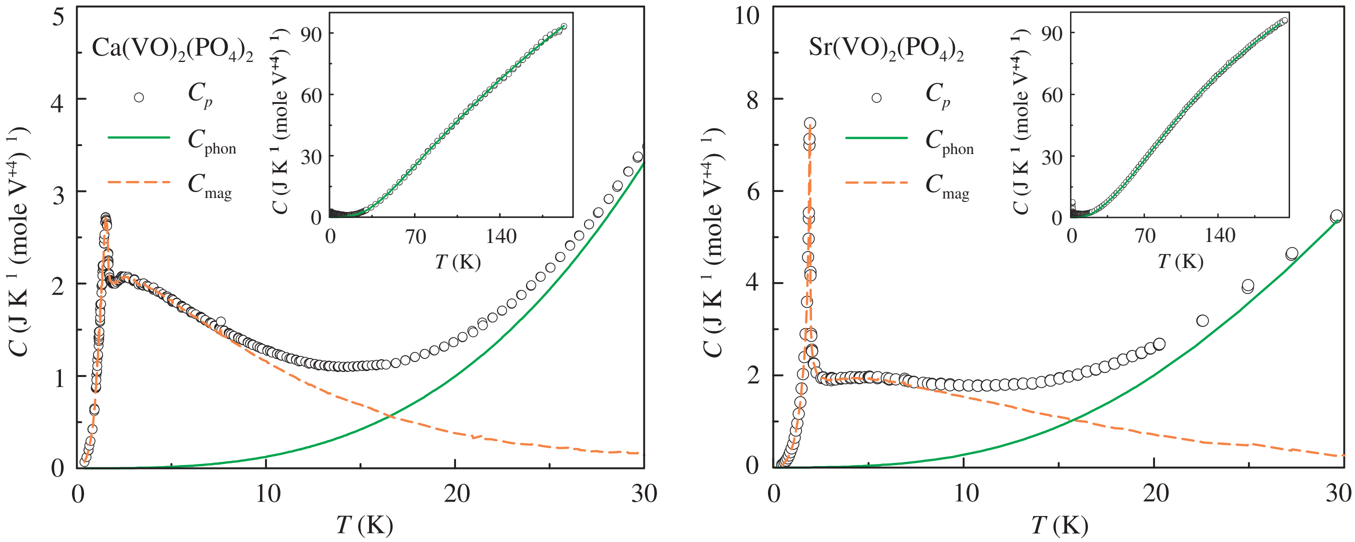

FIG. 4: (Color online) Temperature dependence of the specific heat measured at zero field for $Ca(VO)_2(PO_4)_2$ (left panel) and $Sr(VO)_2(PO_4)_2$ (right panel). The open circles are the raw data, the solid lines show the phonon contribution C_{phon} as found from the fit to Eq. (2), and the dashed lines denote the magnetic contribution C_{mag}. The insets show the fits with Eq. (2) in the wide temperature range.

lattice shows a high $C_{\text{mag}}^{\max} \simeq 0.46R$.[34,35] In the 1D case, $C_{\text{mag}}^{\max}$ is decreased to $0.35R$ due to stronger quantum fluctuations.[30,34] The triangular lattice (a frustrated 2D system) shows an even lower ($C_{\text{mag}}^{\max} = 0.22R$) and broader maximum as compared to the uniform chain.[34]

According to the results of band structure calculations (Sec. V), the spin systems of $M(VO)_2(PO_4)_2$ are 3D. The high dimensionality should result in a narrow maximum of the magnetic specific heat with a high absolute value at the maximum. However, the $M(VO)_2(PO_4)_2$ compounds reveal broad maxima with the absolute values of about $0.25R$ and $0.23R$ for M = Ca and Sr, respectively. Such absolute values are well below that for the uniform chain (1D non-frustrated system) and nearly match the value for the triangular lattice (2D frustrated system). This result points to the presence of strong quantum fluctuations in the $M(VO)_2(PO_4)_2$ compounds. The spin systems are 3D; therefore the fluctuations should be entirely caused by the frustration. The different breadth of the maxima for the calcium and strontium compounds (see Fig. 5) may also be an indication of the stronger frustration in $Sr(VO)_2(PO_4)_2$.

The strong frustration evidenced by the specific heat data is consistent with the considerable reduction in the ordering temperature T_N as compared to $T_{\max}^{\chi}$ (see the previous subsection). However, in contrast to the geometrically frustrated systems, T_N does not vanish completely, and at sufficiently low temperatures, long-range magnetic ordering is established. To understand the nature of the ordered state, we studied field dependence of the specific heat (Fig. 6). At large, the transition temperature gradually decreases with the increase in the field and finally gets suppressed below 0.4 K at 8 and 11.5 T for $Ca(VO)_2(PO_4)_2$ and $Sr(VO)_2(PO_4)_2$, respectively.[36] The $H-T$ phase diagrams shown in the insets of Fig. 6 are typical for antiferromagnets and point to antiferromagnetic ordering in the $M(VO)_2(PO_4)_2$ compounds.

C. ^{31}P NMR

For both the compounds, the ^{31}P NMR spectra consist of a single and narrow spectral line as is expected for $I = 1/2$ nuclei.[37,38] The single spectral line implies

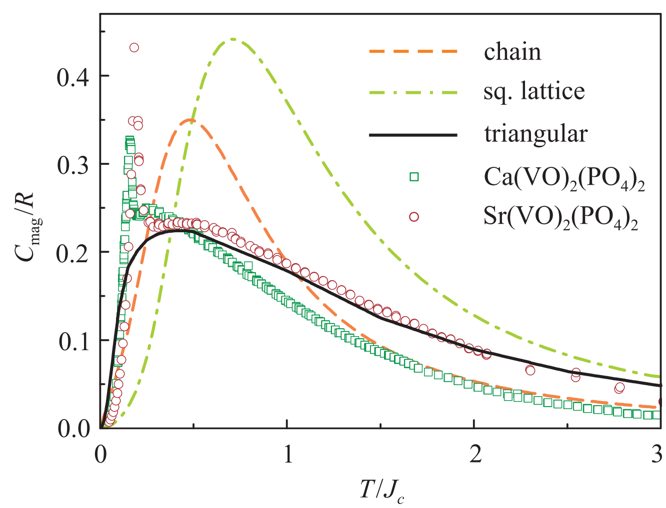

FIG. 5: (Color online) Magnetic contribution to the specific heat of $M(VO)_2(PO_4)_2$ and theoretical curves for the uniform chain (Refs. 30 and 34), non-frustrated square lattice (Refs. 34 and 35), and triangular lattice (Ref. 34) models. The reduced temperature scale T/J_c with $J_c = \sqrt{\sum_i J_i^2}$ is used.

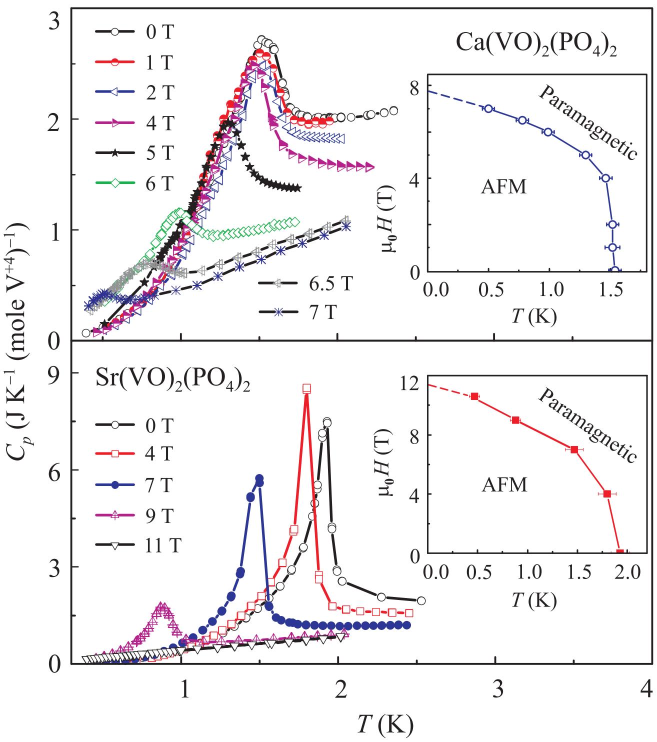

FIG. 6: (Color online) Specific heat of $Ca(VO)_2(PO_4)_2$ (upper panel) and $Sr(VO)_2(PO_4)_4$ (bottom panel) measured at different applied fields (H). The insets show the respective $H-T$ phase diagrams.

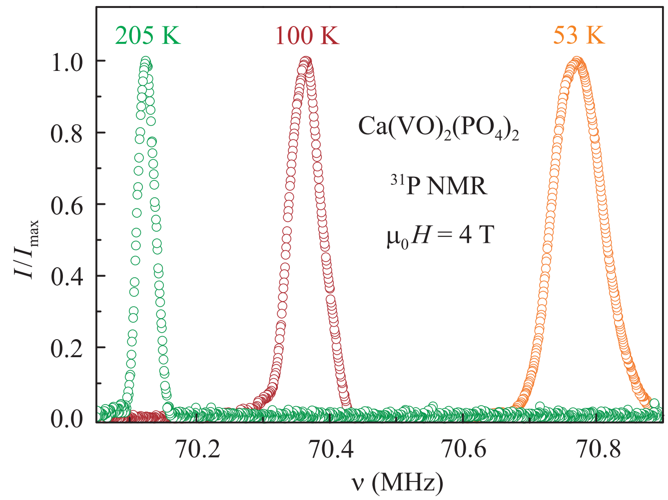

FIG. 7: (Color online) ^{31}P NMR spectra for $Ca(VO)_2(PO_4)_2$ measured at 4 T by the Fourier transform of the spin-echo signal above T_N. The representative spectra show the line shift with temperature. All the spectra are normalized to unity by dividing the intensity (I) by the maximum intensity ($I_{\max}$).

that both $Ca(VO)_2(PO_4)_2$ and $Sr(VO)_2(PO_4)_2$ have a unique ^{31}P site consistent with the structural data. Additionally, narrow line is also a signature of good sample quality. Figure 7 shows the representative spectra for $Ca(VO)_2(PO_4)_2$ above the transition temperature. The line width and the line shift were found to be temperature dependent.

The temperature dependence of the NMR shift $K(T)$ (Fig. 8) behaves similar to the bulk susceptibility χ (see Fig. 2). NMR has an important advantage over χ for the determination of magnetic parameters. At low temperatures, extrinsic Curie-type paramagnetic contribution often affects the bulk susceptibility, while in case of NMR this contribution broadens the spectral line but does not contribute to the line shift. Therefore, it is sometimes more reliable to extract the magnetic parameters from the temperature dependence of the NMR shift rather than from the bulk susceptibility.

The hyperfine Hamiltonian for ^{31}P can be written in the form $\hat{H} = -\gamma\hbar \mathbf{I} A_{hf} \mathbf{S}$, with $\mathbf{I}$ and $\mathbf{S}$ being dimensionless nuclear and electron spins, respectively. The NMR shift K is a direct measure of the uniform spin susceptibility $\chi_{\rm spin}$. Quite generally, their relation is written as follows:

$$K = \delta + \left(\frac{A_{hf}}{N_A \mu_B}\right)\chi_{\rm spin} \tag{4}$$

where δ is the temperature-independent chemical shift, which is almost negligible, N_A is the Avogadro constant, and A_{hf} is the transferred hyperfine coupling between the electrons and the probing nuclei. Therefore to calculate A_{hf}, one should use K vs. $\chi_{\rm spin}$ plot with T as an implicit parameter. Since above 3 K the extrinsic paramagnetic contribution is negligible for both the compounds, we use the bulk susceptibility χ instead of the spin susceptibility $\chi_{\rm spin}$. The resulting plots are shown in Fig. 9. The fits yield $A_{hf} = (4920\pm200)$ and (5125 ± 200) Oe/μ_B for $Ca(VO)_2(PO_4)_2$ and $Sr(VO)_2(PO_4)_2$, respectively. The linearity of the K vs. $\chi_{\rm spin}$ plots confirms that by measuring $K(T)$ we can trace $\chi_{\rm spin}(T)$ properly. The obtained hyperfine couplings for ^{31}P are of the same order as the values previously reported for vanadium phosphates[39,40,41] and indicate a sizeable hybridization of P and V orbitals mediated by $2p$ orbitals of oxygen.

To extract the magnetic parameters, we fitted $K(T)$ curves above 15 K with the Curie-Weiss law $\chi = C/(T + \theta_{\rm CW})$. The resulting values of the effective moment ($\mu_{\rm eff}^K$) and the Curie-Weiss temperature ($\theta_{\rm CW}^K$) are listed in Table I. These values are in good agreement with that obtained from the analysis of the bulk susceptibility.

For the $1/T_1$ experiment, the frequencies of the central positions of the corresponding spectra at 70 MHz have been excited. For a spin-1/2 nucleus, the longitudinal magnetization recovery is expected to follow a single exponential behavior. In $M(VO)_2(PO_4)_2$, the recovery of the nuclear magnetization after an inverting pulse can indeed be described by a single exponential, $\frac{1}{2}\left(\frac{M(\infty)-M(t)}{M(\infty)}\right) = A_1 \exp\left(-t/T_1\right) + C$, where $M(t)$ is the nuclear magnetization at a time t after an inverting pulse, while A_1 and C are time-independent constants. Temperature dependences of $1/T_1$ are pre-

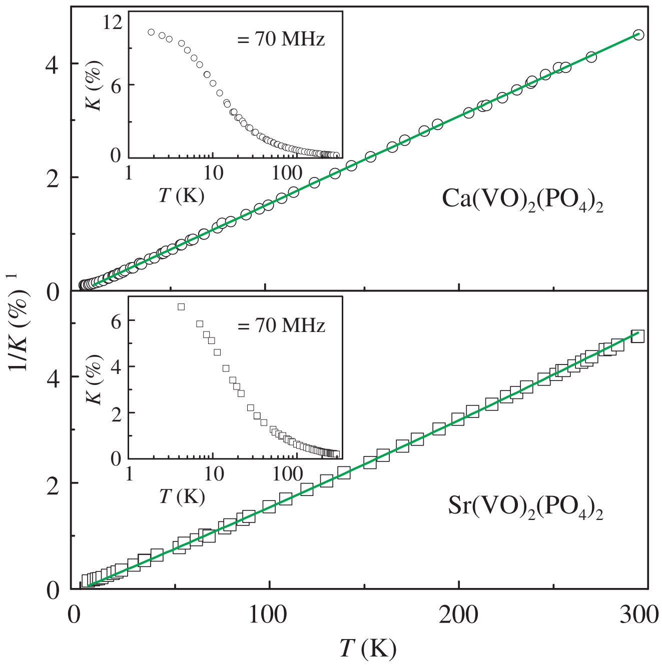

FIG. 8: (Color online) Inverse of [31]P NMR shift ($1/K$) vs. T for $Ca(VO)_2(PO_4)_2$ (upper panel) and $Sr(VO)_2(PO_4)_2$ (bottom panel). Circles and squares indicate the experimental data, while the solid lines show the Curie-Weiss fits. The insets present the K vs. T curves.

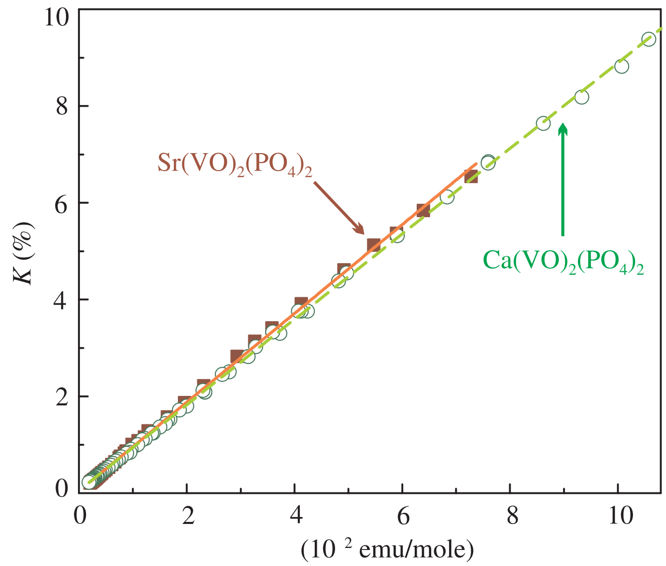

FIG. 9: (Color online) [31]P NMR shift (K) vs. bulk susceptibility (χ) with temperature as an implicit parameter. We employ the χ data collected at the applied field of 4 T, since this field was used for the NMR measurements. The solid and dashed lines show the linear fits with Eq. (4).

sented in Fig. 10. The spin-lattice relaxation rates are temperature-independent above 20 K and rapidly increase with the reduction in temperature below 20 K. The temperature-independent behavior of $1/T_1$ is typical for the paramagnetic regime with fast and random fluctuations of electronic spins.[42] The critical divergence in the vicinity of T_N corresponds to the slowing down of fluctuating moments and indicates the approach to the state with long-range magnetic ordering.

Furthermore, the $1/T_1$ data enable to estimate exchange couplings in the system under investigation. According to Moriya,[42] the high-temperature limit of $1/T_1$ for a system of localized moments can be expressed as follows:

$$\left(\frac{1}{T_1}\right)\bigg|_{T\to\infty} = \frac{\gamma^2}{2}\frac{S(S+1)}{3}\frac{\sqrt{2\pi}}{\omega_{\mathrm{E}}} \times \sum_{k,i,j} |A_{ij}^k|^2 \qquad (5)$$

where A_{ij}^k ($i,j = x,y,z$) are the components of the hyperfine tensor due to the k^{th} magnetic atom. The Heisenberg exchange frequency ω_{E} is defined as $\omega_{\mathrm{E}} = J_c(k_B/\hbar)\sqrt{2zS(S+1)/3}$, $J_c = \sqrt{\sum_i J_i^2}$ is the thermodynamic energy scale of the exchange couplings, and $z = z_i = 2$ (as introduced in Sec. IV B).[19] Using the relevant parameters and the experimental high-temperature relaxation rates 8 and 8.5 ms^{-1} (see Fig. 10), we find $J_c^{T_1} \simeq$ 13.4 and 14.1 K for $Ca(VO)_2(PO_4)_2$ and $Sr(VO)_2(PO_4)_2$, respectively. These values are in reasonable agreement with the estimates $J_c^C \simeq 10$ K from the specific heat (see Sec. IV B).

In the spectral measurements at low temperatures (slightly above T_N), a broad background signal appears along with the central peak for both the compounds. At T_N, the central peak vanishes, and the broad background signal becomes prominent extending over a large field range of about 5 T. This effect is illustrated in the inset of Fig. 10 for $Sr(VO)_2(PO_4)_2$. The central line disappears at 1.7 K consistent with the ordering temperature of 1.8 K as determined by the specific heat measurements (see the inset of Fig. 6 and note that we use the T_N value at 4 T, since the NMR measurements are carried out at this applied field). The broadening of our spectra upon approaching T_N from above is the usual behavior expected for the magnetic ordering. Below T_N, the spectral intensity melts into a broad background signal which gives strong evidence of a large distribution of internal static fields in the ordered state. Similar broadening of the spectral line has been observed for many other materials in the magnetically ordered state (see, e.g., Refs. 43 and 44).

V. BAND STRUCTURE

The $M(VO)_2(PO_4)_2$ compounds reveal quite complicated spin systems with numerous superexchange paths; therefore the presented experimental data do not allow to determine the individual exchange couplings unambiguously. To overcome this difficulty, we turn to band structure calculations, estimate individual exchange couplings and construct a microscopic model of the exchange

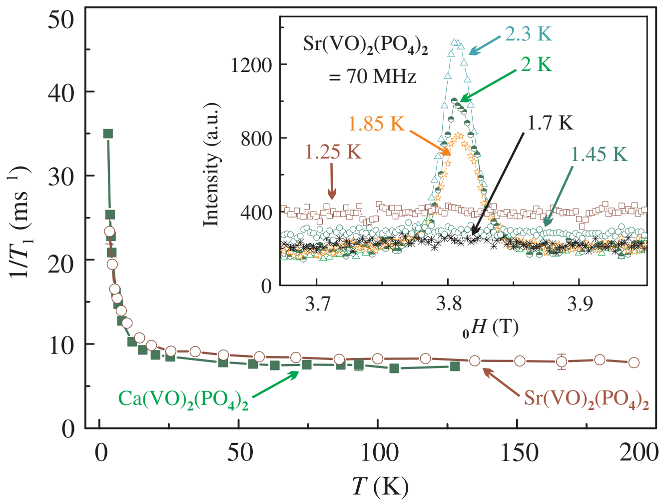

FIG. 10: (Color online) Spin-lattice relaxation rate ($1/T_1$) vs. temperature (T) for the $M(VO)_2(PO_4)_2$ compounds. The inset shows the field sweep spectra of $Sr(VO)_2(PO_4)_2$ measured at the transmitter frequency of 70 MHz and temperatures close to T_N.

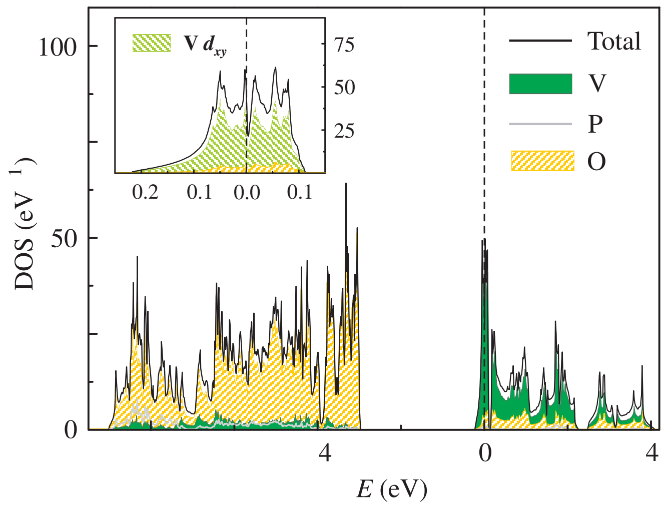

FIG. 11: (Color online) LDA density of states for $Ca(VO)_2(PO_4)_2$. The Fermi level is at zero energy. The calcium contribution is negligible in the whole energy range, therefore it is not presented in the figure. The inset zooms the image near the Fermi level, only V $3d_{xy}$ and oxygen contributions are shown.

interactions. As we will show below, the computational analysis of the $M(VO)_2(PO_4)_2$ compounds is also rather difficult, and one can hardly expect the reliable quantitative estimates of all the exchange couplings in the systems under investigation. Nevertheless, we succeed to establish a reasonable spin model and provide a plausible explanation of the frustration (Sec. VI).

Experimental data show the similarity of the magnetic properties of the $M(VO)_2(PO_4)_2$ compounds with M = Ca and Sr. We calculated band structures for both the compounds, analyzed exchange couplings and did not find any considerable differences between the two systems. Therefore, in the following we will discuss the calcium compound only. The whole discussion is applicable to $Sr(VO)_2(PO_4)_2$ as well.

A. LDA and tight-binding model

The LDA density of states plot for $Ca(VO)_2(PO_4)_2$ is shown in Fig. 11. Valence bands below -3 eV are mainly formed by oxygen orbitals, while the states near the Fermi level have predominantly vanadium character with an admixture of oxygen. The phosphorous and calcium contributions to these states are tiny and hardly visible in the figure. Note that the energy spectrum is gapless in evident contradiction with the green color of $Ca(VO)_2(PO_4)_2$. This is a typical failure of LDA due to an underestimate of strong electron-electron correlations in the V $3d$ shell. Local spin density approximation (LSDA)+U calculations readily reproduce the insulating spectrum with an energy gap of $2.5-2.8$ eV. The latter values are in reasonable agreement with the sample color.

TABLE II: The hopping parameters t_i of the tight-binding model and the resulting antiferromagnetic couplings J_i^{AFM} for $Ca(VO)_2(PO_4)_2$. Only the interactions involving PO_4 tetrahedra are listed. The effective on-site Coulomb repulsion potential $U_{\mathrm{eff}} = 4.5$ eV.

	t_1	t_2	t_3	t_4	t_5
t (meV)	-12	-33	36	-3	-3
	J_1	J_2	J_3	J_4	J_5
J^{AFM} (K)	1.5	11.3	13.4	0.1	0.1

To study exchange interactions, we construct an effective model that includes the relevant, half-filled bands only. Thus, we focus on the bands that are close to the Fermi level and have predominantly vanadium character. According to the discussion in Sec. II, distorted octahedral coordination of vanadium gives rise to a non-degenerate d_{xy} ground state. Indeed, we find four bands formed by V d_{xy} orbitals in the energy range between -0.2 and 0.1 eV (see the inset of Fig. 11 and Fig. 12). These bands correspond to four vanadium atoms in the primitive cell of $Ca(VO)_2(PO_4)_2$ and are used for a tight-binding fit of the transfer integrals (hoppings) relevant for the AFM exchange interactions. The resulting transfer integrals (t) are introduced to the extended Hubbard model, and the correlation effects are taken into account explicitly via an effective on-site repulsion potential U_{eff}.[45] In our case $t \ll U_{\mathrm{eff}}$, hence the Hubbard model at half-filling can be reduced to a Heisenberg model for the low-lying (i.e., spin) excitations. Thus, we are able to estimate AFM contributions to the exchange couplings as $J_i^{\mathrm{AFM}} = 4t_i^2/U_{\mathrm{eff}}$. Similar to Ref. 25, we use $U_{\mathrm{eff}} = 4.5$ eV – a representative value for vanadium oxides.

An advantage of the TB approach is the possibility to estimate all the exchange couplings in the system under investigation. Yet the TB fit is sometimes non-unique, and this is the case for $Ca(VO)_2(PO_4)_2$ due to the presence of numerous NN and NNN hoppings. To get an unambiguous solution, we assume that the leading interactions run via PO_4 tetrahedra (i.e., correspond to $t_1 - t_5$ introduced in Sec. II). This assumption looks reasonable, since magnetic interactions in transition metal phosphates are usually mediated by PO_4 groups (see, e.g., Refs. 25, 32, 38, and 46). Moreover, phosphorous gives larger contribution to the states near the Fermi level as compared to calcium. Thus, the V–O–P–O–V superexchange paths should be favorable.

The resulting TB fit is in perfect agreement with the LDA band structure (see Fig. 12). Table II lists the hoppings involving PO_4 tetrahedra and the respective exchange integrals.[47] The strongest AFM coupling runs between non-parallel structural chains (J_3), the other strong coupling occurs between parallel chains (J_2), and all the other AFM couplings are weaker at least by a factor of eight. The magnitude of $J's$ is consistent with the experimental data, although the precise values are somewhat overestimated. For example, considering J_2 and J_3 only, we find $J_c = 17.7$ K that slightly exceeds the $J_c^{T_1} \approx 13$ K estimate from NMR and is well above the estimate $J_c^C \approx 10$ K from the specific heat.

B. LSDA+U, results

The spin system formed by J_2 and J_3 is 3D and non-frustrated. To get a frustrated scenario, one has to consider additionally FM interactions using LSDA+U calculations. The regular approach deals with the construction of a supercell enabling different patterns of spin ordering, the mapping of the resulting energies onto a Heisenberg model, and the estimate of individual exchange integrals (see, e.g., Ref. 25). However, this approach seems to be inappropriate for $Ca(VO)_2(PO_4)_2$, as the magnetic interactions are very weak, and the change in the total energy due to the variation of spin ordering is of the order of 10 K (i.e., 10^{-5} Hartree or $\sim 10^{-9}$ of the total energy). Thus, we have to use the smallest unit cell in order to achieve the highest possible accuracy, and only sums of the exchange couplings can be estimated. Nevertheless, one may expect that the TB results on J_i^{AFM} will enable to resolve FM interactions (at least, qualitatively).

The results of the LSDA+U calculations are listed in Table III. The most stable spin configuration is formed by ferromagnetic structural chains that are coupled both ferromagnetically (for parallel chains) and antiferromagnetically (for non-parallel chains). We find the same ground state for $U_d = 4 - 6$ eV, although the exchange couplings strongly depend on the U_d value. This problem will be addressed below (Sec. V C) after a comparison of the LSDA+U results with the experimental data and the TB estimates.

TABLE III: LSDA+U estimates for the exchange integrals in $Ca(VO)_2(PO_4)_2$ and the resulting Curie-Weiss temperatures $\theta_{\mathrm{CW}}^{\mathrm{calc}}$.

U_d (eV)	$J_1 + J_2$ (K)	J_3 (K)	$J_4 + J_5$ (K)	$\theta_{\mathrm{CW}}^{\mathrm{calc}}$ (K)
4	2.9	4.4	6.0	6.7
5	−14.0	4.1	9.2	−0.4
6	−40.5	3.7	14.0	−11.4

As we have mentioned in Sec. III, U_d is an adjustable parameter that depends on the basis set, crystal structure of the compound under investigation, and the objective parameters of the calculation. Usually, one has to fit U_d to some observable quantity (energy gap, magnetic moments, etc.). It is preferable to use the quantity that is related to the objective parameters, since different objective parameters may require the application of different U_d values. Below, we will employ the Curie-Weiss temperature θ_{CW} for this purpose. The Curie-Weiss temperature is the second-order term in the high-temperature series expansion of the magnetic susceptibility. According to Ref. 30, for spin-1/2 system $\theta_{\mathrm{CW}} = 1/4 \sum_i z_i J_i = 1/2 \sum_i J_i$. Thus, θ_{CW} is directly related to the exchange couplings and provides reasonable justification for the choice of the U_d value.

Clearly, the results for $U_d = 5$ eV are in good agreement with the experimental estimate $\theta_{\mathrm{CW}} \simeq -0.3$ K, while for $U_d = 4$ and 6 eV the compliance of the experimental and computational results is quite poor (see Table III). Thus, the optimal value of U_d for $Ca(VO)_2(PO_4)_2$ is 5 eV.[48] Yet in contrast to other spin-

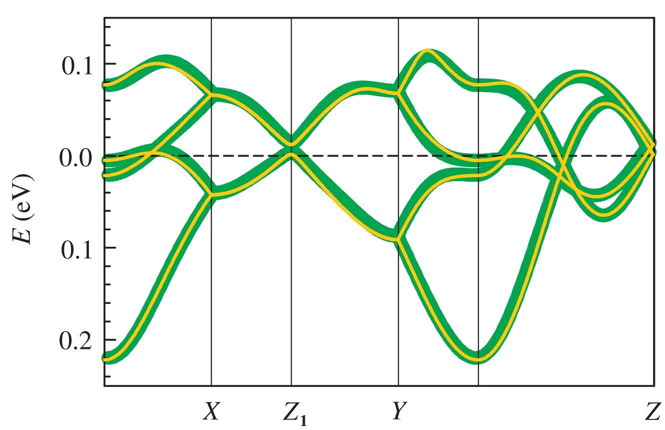

FIG. 12: (Color online) LDA band structure of $Ca(VO)_2(PO_4)_2$ near the Fermi level (thin light lines) and the fit with the tight-binding model (thick darker lines). The Fermi level is at zero energy. The notation of k points is as follows: $\Gamma(0,0,0)$, $X(0.5,0,0)$, $Z_1(0.5,0.5,0)$, $Y(0,0.5,0)$, and $Z(0,0,0.5)$ (the coordinates are given along k_x, k_y, and k_z in units of the respective reciprocal lattice parameters $4\pi/a$, $4\pi/b$, and $4\pi/c$). The points Z and Z_1 are equivalent due to the face-centered symmetry of the unit cell.

1/2 systems,[8,25,46] the slight variation of U_d results in a huge change in the exchange couplings (see Table III). This effect will be further discussed in Sec. V C. In the rest of this subsection, we will focus on the exchange couplings calculated with $U_d = 5$ eV.

According to Tables II and III, $J_1+J_2 \ll J_1^{\mathrm{AFM}}+J_2^{\mathrm{AFM}}$ indicating considerable FM contribution to either J_1 and/or J_2. J_3 is smaller than J_3^{AFM} and positive, hence there is also a FM contribution to J_3, but the overall interaction remains AFM. Finally, $J_4+J_5 \gg J_4^{\mathrm{AFM}}+J_5^{\mathrm{AFM}}$, i.e., the LSDA+$U$ and TB estimates for these couplings are inconsistent. One may think that additional interactions contribute to the LSDA+U value of $J_4 + J_5$, but such contributions yield $2-3$ K only[49] and do not explain the controversy. Our experience shows that the TB approach is highly reliable for estimating exchange couplings in spin-1/2 systems.[25,46,50] In contrast to LSDA+U, the TB approach includes a simple explicit relation between J_i and U_{eff}, while the underlying LDA calculation is *ab initio* and does not include any adjustable parameters. Therefore, we have to admit the failure of LSDA+U to provide valid quantitative estimates of the weak exchange couplings in $Ca(VO)_2(PO_4)_2$ (see Sec. V C for further discussion). Nevertheless, the LSDA+U results are helpful to get a qualitative understanding of the system under investigation.

To get an idea about the FM interactions in $Ca(VO)_2(PO_4)_2$, we consider vanadium–vanadium separations for $J_1 - J_3$. The shortest separation (3.46 Å) corresponds to J_1, while J_2 and J_3 reveal larger distances of 6.15 and 4.35 Å, respectively. FM interactions are short-range; therefore it is natural to suggest the strongest FM contribution to be that of J_1. Since J_1^{AFM} is close to zero, the overall interaction J_1 should be FM. Unlike J_1, J_2 and J_3 are AFM, although the FM contributions may also be non-negligible and reduce the absolute values of the exchange couplings. The presence of the ferromagnetic in-chain interaction J_1 is consistent with our studies of other vanadium phosphates having similar chains of corner-sharing octahedra.[51]

Thus, the basic microscopic model for $Ca(VO)_2(PO_4)_2$ includes three exchange couplings: ferromagnetic J_1 and antiferromagnetic J_2 and J_3 interactions. The resulting spin system is 3D and frustrated (see Fig. 13 and Sec. VI). Unfortunately, the computational results do not enable quantitative estimates of individual exchange couplings (see the above discussion and Sec. V C). Therefore, we do not make further numerical comparisons with the experimental data. Clearly, the presence of both the FM and AFM couplings is qualitatively consistent with the strongly reduced θ_{CW}. Moreover, band structure calculations suggest rather weak (about 10 K) exchange interactions in $Ca(VO)_2(PO_4)_2$ consistent with the experimental energy scale $J_c = 10-15$ K. We are convinced that the agreement between the band structure results and the experimental data is reasonable, especially taking into account the complexity of the spin system and the weakness of the exchange couplings.

C. LSDA+U: The influence of U_d

To understand the J vs. U_d trends, one should consider exchange integrals as composed of the AFM and FM contributions: $J = J^{\mathrm{AFM}} + J^{\mathrm{FM}}$. Within one-band Hubbard model, $J^{\mathrm{AFM}} \sim t^2/U$, while J^{FM} is independent of U. Therefore, the overall J should be reduced with the increase in U. The repulsion potential U_d is a parameter of the computational method rather than the true on-site Coulomb repulsion, and J^{AFM} is not necessarily proportional to $1/U_d$. Yet the increase in U_d tends to improve the localization of $3d$ electrons hence suppressing AFM interactions. Thus, one would expect that antiferromagnetic exchange couplings should be reduced with the increase of U_d. In fact, the strongest coupling usually shows $\sim 1/U_d$ behavior, while other exchange integrals are nearly independent of U_d (see, e.g., Refs. 25 and 52). If $J^{\mathrm{AFM}} \gg J^{\mathrm{FM}}$, the overall J is antiferromagnetic for any reasonable value of U_d. However, for small $J^{\mathrm{AFM}} \approx J^{\mathrm{FM}}$ the situation will be different, and the resulting J may be positive for small U_d and negative for large U_d.

The above considerations naturally explain, why FM interactions manifest themselves (hence reducing θ_{CW}) at $U_d \geq 5$ eV only. However, the FM interactions are further enhanced with the increase in U_d, and this effect has a different origin. LSDA+U treats electronic correlations within mean-field approximation; therefore the filled states of vanadium are merely shifted to lower energies as the repulsive potential U_d is applied. At lower energies, oxygen states dominate; hence vanadium–oxygen hybridization is enhanced with the increase in U_d. Indeed, our calculations reveal the decrease in the magnetic moment of vanadium and the partial spin polarization of oxygen atoms as U_d is increased. In case of $Ca(VO)_2(PO_4)_2$, this effect is even more pronounced as compared to other vanadium compounds.[25,52] Moreover, the exchange couplings are very weak, and the overestimated vanadium–oxygen hybridization results in unrealistic results for J_i (note the $J_1 + J_2$ value of -40 K at $U_d = 6$ eV).

In summary, we should point to two complications that arise during LSDA+U calculations for vanadium oxides with very weak magnetic interactions. First, one has to apply a relatively large U_d in order to suppress AFM couplings and to reveal FM contributions. Second, large U_d tends to overestimate vanadium–oxygen hybridization and to produce unrealistic enhancement of the exchange couplings. There is an optimal U_d value [5 eV in case of $Ca(VO)_2(PO_4)_2$] that gives rise to a reasonable solution. However, even at this value both problems are retained. In general, we think that LSDA+U estimates of weak exchange couplings in highly complex structures are not accurate enough to provide quantitatively correct results. Therefore, we mainly rely on the TB model in our analysis. Nevertheless, LSDA+U estimates facilitate a qualitative understanding of the coupling scenario resulting in a reasonable microscopic description of the

magnetic behavior.

VI. DISCUSSION

Our experimental results show that the complex vanadium phosphates $M(VO)_2(PO_4)_2$ are strongly frustrated spin systems with competing FM and AFM exchange couplings. Magnetic susceptibility data reveal a maximum at $T^{\chi}_{\max} \simeq 3$ K and nearly vanishing Curie-Weiss temperatures $\theta_{\rm CW} \leq 1$ K. For simple spin systems with a single leading exchange coupling, $T^{\chi}_{\max}$ and $\theta_{\rm CW}$ are usually close to each other, while the $\theta_{\rm CW} \ll T^{\chi}_{\max}$ regime implies the presence of several different magnetic interactions in the system under investigation. As we have stated above, $\theta_{\rm CW}$ is equal to half of the sum of all the exchange integrals. Thus, the low $\theta_{\rm CW}$ value points to the presence of both FM and AFM interactions that compensate each other. Further on, the low Néel temperatures ($T_N \approx T^{\chi}_{\max}/2$) indicate that long-range ordering in the system is impeded by either low dimensionality and/or magnetic frustration.

Low-temperature specific heat provides the information on the spin excitations and presents one of the substantial characteristics of quantum magnets. In systems with strong quantum fluctuations, the specific heat maximum is reduced due to the suppression of correlated spin excitations. The maximum of the magnetic specific heat of the $M(VO)_2(PO_4)_2$ compounds ($C^{\max}_{\rm mag}$) equals to $0.25R$ only. This value is comparable to that for the spin-1/2 triangular lattice, a system with strong geometrical frustration, and lies well below $C^{\max}_{\rm mag}$ typical for non-frustrated low-dimensional spin systems. Thus, strong quantum fluctuations are present in $M(VO)_2(PO_4)_2$, and these fluctuations are likely caused by the magnetic frustration.

To reveal the origin of the frustration in the $M(VO)_2(PO_4)_2$ compounds, we have performed band structure calculations and estimated the individual exchange couplings. Despite the problems discussed in Sec. V C, we succeeded to construct a reasonable microscopic model that provides a plausible scenario of the frustration. The coupling within the structural chains (the chains of corner-sharing VO_6 octahedra, see Fig. 1) is FM (J_1), while interchain couplings are AFM (J_2 and J_3). The interactions form a quadrangle with one FM and three AFM sides (Fig. 13). The FM in-chain interaction favors the parallel alignment of the spins within the chain, while the inter-chain AFM interactions favor the antiparallel alignment. Thus, the spin system is frustrated.

Below, we will use several experimental quantities ($\theta_{\rm CW}, J_c$, and H_s) in order to estimate the individual exchange couplings of the proposed model. Assuming the ground state revealed by the LSDA+U calculations (see Sec. V B), we find $H_s = 2J_3 g\mu_B/k_B$ (the Heisenberg model is treated in a classical way). Using the averaged estimates of $J_c = (J_c^C + J_c^{T_1})/2$ and

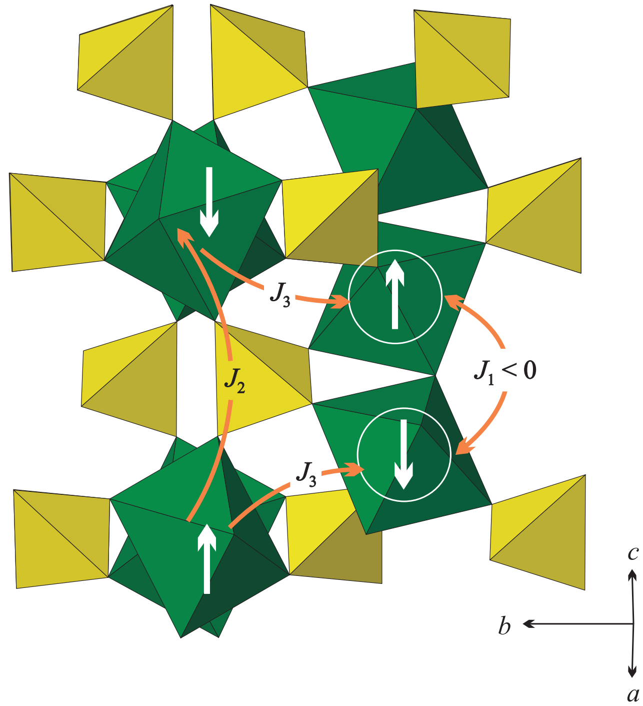

FIG. 13: (Color online) Enlargement of the crystal structure of $Ca(VO)_2(PO_4)_2$ (see Fig. 1) that shows the proposed scenario of the frustration. Antiferromagnetic inter-chain couplings J_2, J_3 favor antiparallel orientation of spins for neighboring atoms in the chain (marked by large circles), while the in-chain coupling (J_1) is ferromagnetic and would favor parallel alignment of the respective spins.

$\theta_{\rm CW} = (\theta^{\chi}_{\rm CW} + \theta^{K}_{\rm CW})/2$ and assuming negative J_1, one arrives at $J_1 = -9.6$ K, $J_2 = 3.5$ K, and $J_3 = 5.4$ K for $Ca(VO)_2(PO_4)_2$ and $J_1 = -8.9$ K, $J_2 = 1.8$ K, and $J_3 = 7.7$ K for $Sr(VO)_2(PO_4)_2$. These values should be considered as rough estimates, since our model includes three interactions only, and the results of different methods for J_c and $\theta_{\rm CW}$ are simply averaged. The estimates emphasize the similarity of the calcium and strontium compounds, although J_2 and J_3 values are somewhat different for M = Ca and Sr. The latter result may be relevant for the different breadth of the specific heat maxima in the two compounds (see Fig. 5).

We should emphasize that at least two couplings (J_1 and J_3) in the $M(VO)_2(PO_4)_2$ compounds have similar magnitude, and the spin system is essentially 3D rather than 1D with frustrated inter-chain couplings. The frustration is controlled by the magnitudes of the competing exchange interactions. For example, the decrease of the absolute value of J_1 will reduce the frustration, while for AFM J_1 the system is non-frustrated at all. To the best of our knowledge, no theoretical results for this model are available. Basically, one may expect the presence of strongly frustrated regions [one is revealed by the $M(VO)_2(PO_4)_2$ compounds] and quantum critical points in the respective phase diagram. Further studies of the model and the appropriate materials are desirable.

Finally, we will focus on the structural aspects of the present study. The main structural feature of the $M(VO)_2(PO_4)_2$ compounds deals with the chains of corner-sharing VO_6 octahedra. Such chains are typical for a wide variety of vanadium oxides.[53] Within a very straight-forward and naive approach, one can identify the chains of vanadium polyhedra as spin chains and arrive at 1D spin system with weak inter-chain couplings. According to Sec. II, such an approach is inconsistent with the orbital state of vanadium, and the actual spin system may have any dimensionality depending on the exchange couplings via PO_4 tetrahedra or other side groups. In the case of $M(VO)_2(PO_4)_2$, the actual spin system is 3D. Yet in $Sr_2VO(VO_4)_2$ the spin system is 1D (consistent with the naive expectations), but the spin chains are perpendicular to structural ones (in contrast to the naive expectations).[26] In general, the structures formed by VO_6 octahedra and non-magnetic tetrahedral groups (PO_4, $V^{+5}O_4$, SiO_4, etc.) provide a promising way for studying different spin systems, and further investigations could be interesting. However, we should point to the importance of careful thermodynamic measurements and electronic-structure-based microscopic modeling for proper understanding of the respective systems. Thus, the interesting physics of the $M(VO)_2(PO_4)_2$ compounds is well hidden behind the 1D features of the crystal structure and weak magnetic interactions resulting in the paramagnetic behavior above $4-5$ K. Only the combination of experimental and computational approaches enables us to unravel the relevant microscopic mechanisms and to achieve an insight of the underlying physics.

In conclusion, we have shown that the $M(VO)_2(PO_4)_2$ compounds reveal strongly frustrated 3D spin systems with competing FM and AFM interactions. The presence of both FM and AFM interactions is indicated by the vanishing Curie-Weiss temperature θ_{CW}, while the strong frustration is evidenced by the reduced maximum of the magnetic specific heat. The thermodynamic energy scale of the exchange couplings is $J_c = 10-15$ K as shown by the specific heat and NMR data. Band structure calculations suggest a plausible scenario of the frustration with the FM interaction along the structural chains and the AFM interactions between the chains. In the resulting three-dimensional spin system, the frustration is controlled by the magnitudes of the competing exchange couplings. The proposed spin model deserves further experimental and theoretical studies.

Acknowledgments

The authors are grateful to P. Carretta for his critical suggestions on the NMR results and to Nic Shannon for the fruitful discussions. Financial support of GIF (Grant No. I-811-257.14/03), RFBR (Grant No. 07-03-00890), and the Emmy-Noether program of the DFG as well as the computational facilities of ZIH Dresden are acknowledged.

---

* Electronic address: ramesh˙phy2003@yahoo.com
† Electronic address: altsirlin@gmail.com
‡ Present address: Low Temperature Group, Bariloche Atomic Centre – National Commission of Atomic Energy. Av. Bustillo 9500 (C. P. 8400) S. C. de Bariloche, Argentine.

[1] P. W. Anderson, Science **235**, 1196 (1987).
[2] S. Park, Y. J. Choi, C. L. Zhang, and S.-W. Cheong, Phys. Rev. Lett. **98**, 057601 (2007).
[3] J. E. Greedan, J. Mater. Chem. **11**, 37 (2001).
[4] A. Harrison, J. Phys.: Condens. Matter **16**, S553 (2004).
[5] M. Hase, I. Terasaki, K. Uchinokura, Phys. Rev. Lett. **70**, 3651 (1993).
[6] G. Castilla, S. Chakravarty, and V. J. Emery, Phys. Rev. Lett. **75**, 1823 (1995).
[7] S.-L. Drechsler, N. Tristan, R. Klingeler, B. Büchner, J. Richter, J. Málek, O. Volkova, A. Vasiliev, M. Schmitt, A. Ormeci, C. Loison, W. Schnelle, and H. Rosner, J. Phys.: Condens. Matter **19**, 145230 (2007), and references therein.
[8] S.-L. Drechsler, O. Volkova, A.N. Vasiliev, N. Tristan, J. Richter, M. Schmitt, H. Rosner, J. Málek, R. Klingeler, A. A. Zvyagin, and B. Büchner, Phys. Rev. Lett. **98**, 077202 (2007); cond-mat/0701741
[9] Y. Naito, K. Sato, Y. Yasui, Y. Kobayashi, Y. Kobayashi, and M. Sato, J. Phys. Soc. Jpn. **76**, 023708 (2007); cond-mat/0611659.
[10] F. Schrettle, S. Krohns, P. Lunkenheimer, J. Hemberger, N. Büttgen, H.-A. Krug von Nidda, A. V. Prokofiev, and A. Loidl, Phys. Rev. B **77**, 144101 (2008); arXiv:0712.3583.
[11] Y. Yasui, Y. Naito, K. Sato, T. Moyoshi, M. Sato, and K. Kakurai, J. Phys. Soc. Jpn. **77**, 023712 (2008); arXiv:0711.1204.
[12] S. Seki, Y. Yamasaki, M. Soda, M. Matsuura, K. Hirota, and Y. Tokura, Phys. Rev. Lett. **100**, 127201 (2008); arXiv:0801.2533.
[13] P. Chandra and B. Doucot, Phys. Rev. B **38**, 9335 (1988).
[14] O. P. Sushkov, J. Oitmaa, and Z. Weihong, Phys. Rev. B **63**, 104420 (2001); cond-mat/0007329.
[15] L. Siurakshina, D. Ihle, R. Hayn, Phys. Rev. B **64**, 104406 (2001).
[16] N. Shannon, B. Schmidt, K. Penc, and P. Thalmeier, Eur. Phys. J. B **38**, 599 (2004); cond-mat/0312160.
[17] N. Shannon, T. Momoi, and P. Sindzingre, Phys. Rev. Lett. **96**, 027213 (2006); cond-mat/0512349.
[18] R. Melzi, P. Carretta, A. Lascialfari, M. Mambrini, M. Troyer, P. Millet, and F. Mila, Phys. Rev. Lett. **85**, 1318 (2000); cond-mat/0005273.
[19] R. Melzi, S. Aldrovandi, F. Tedoldi, P. Carretta, P. Millet, and F. Mila, Phys. Rev. B **64**, 024409 (2001); cond-mat/0101066.
[20] H. Rosner, R. R. P. Singh, W. H. Zheng, J. Oitmaa, S.-L. Drechsler, and W. E. Pickett, Phys. Rev. Lett. **88**, 186405 (2002); cond-mat/0110003.

[21] A. Bombardi, J. Rodriguez-Carvajal, S. Di Matteo, F. de Bergevin, L. Paolasini, P. Carretta, P. Millet, and R. Caciuffo, Phys. Rev. Lett. **93**, 027202 (2004).

[22] E. E. Kaul, H. Rosner, N. Shannon, R. V. Shpanchenko, and C. Geibel, J. Magn. Magn. Mater. **272–276**, 922 (2004).

[23] K. H. Lii, B. R. Chueh, H. Y. Kang, and S. L. Wang, J. Solid State Chem. **99**, 72 (1992).

[24] F. Berrah, A. Leclaire, M.-M. Borel, A. Guesdon, and B. Raveau, Acta Cryst. **C55**, 288 (1999).

[25] A. A. Tsirlin, R. Nath, C. Geibel, and H. Rosner, Phys. Rev. B **77**, 104436 (2008); arXiv:0802.2293.

[26] E. E. Kaul, H. Rosner, V. Yushankhai, J. Sichelschmidt, R. V. Shpanchenko, and C. Geibel, Phys. Rev. B **67**, 174417 (2003); cond-mat/0209409.

[27] K. Koepernik and H. Eschrig, Phys. Rev. B **59**, 1743 (1999).

[28] J. P. Perdew and Y. Wang, Phys. Rev. B **45**, 13244 (1992).

[29] Note that we use FPLO7 in the present work. The basis sets employed in this code are slightly different from that of FPLO5 (applied in Ref. 25). Thus, the use of a different U_d value may be required.

[30] D. C. Johnston, R. K. Kremer, M. Troyer, X. Wang, A. Klümper, S. L. Budko, A. F. Panchula, and P. C. Canfield, Phys. Rev. B **61**, 9558 (2000); cond-mat/0003271.

[31] In the strontium compound, the transition anomaly is more pronounced, and the origin of this effect is not clear. Basically, the specific heat anomalies are affected by both intrinsic (dimensionality of the spin system) and extrinsic (sample quality) factors. At present, we can not distinguish which of these factors are relevant for the difference of the transition anomalies for the $M(VO)_2(PO_4)_2$ compounds.

[32] N. S. Kini, E. E. Kaul, and C. Geibel, J. Phys.: Condens. Matter **18**, 1303 (2006).

[33] R. Nath, A. A. Tsirlin, H. Rosner, and C. Geibel, arXiv:0803.3535.

[34] B. Bernu and G. Misguich, Phys. Rev. B **63**, 134409 (2001); cond-mat/0003381.

[35] M. Hofmann, T. Lorenz, K. Berggold, M. Grüninger, A. Freimuth, G. S. Uhrig, and E. Brück, Phys. Rev. B **67**, 184502 (2003).

[36] The careful inspection of the T_N vs. H dependence reveals slightly different behavior of $Ca(VO)_2(PO_4)_2$ and $Sr(VO)_2(PO_4)_2$ at low fields. The ordering temperature of the calcium compound is nearly field-independent below 4 T, while T_N of the strontium compound is somewhat below the zero-field value even at low fields. In general, one may expect that low fields suppress quantum fluctuations hence increasing T_N (such behavior was observed in another vanadium phosphate, $BaCdVO(PO_4)_2$, see Ref. 33 for details). However, the manifestation of this effect depends on the magnetic anisotropy, the magnitude of quantum fluctuations and, possibly, some extrinsic factors. Thus, the slightly different behavior of the two compounds is explainable, although at present we are unable to suggest a unique reason of the effect.

[37] R. Nath, A. V. Mahajan, N. Büttgen, C. Kegler, A. Loidl, and J. Bobroff, Phys. Rev. B **71**, 174436 (2005); cond-mat/0408530.

[38] R. Nath, D. Kasinathan, H. Rosner, M. Baenitz, and C. Geibel, Phys. Rev. B **77**, 134451 (2008); arXiv:0804.1262.

[39] Y. Furukawa, A. Iwai, K. Kumagai, and A. Yakubovsky, J. Phys. Soc. Jpn. **65**, 2393 (1996).

[40] J. Kikuchi, K. Motoya, T. Yamauchi, and Y. Ueda, Phys. Rev. B **60**, 6731 (1999); cond-mat/9902205.

[41] J. Kikuchi, N. Kurata, K. Motoya, T. Yamauchi, and Y. Ueda, J. Phys. Soc. Jpn. **70**, 2765 (2001); cond-mat/0102365.

[42] T. Moriya, Prog. Theor. Phys. **16**, 23 (1956); *ibid.* **16**, 641 (1956).

[43] J. L. Gavilano, S. Mushkolaj, H. R. Ott, P. Millet, and F. Mila, Phys. Rev. Lett. **85**, 409 (2000); cond-mat/0005534.

[44] P. Vonlanthen, K. B. Tanaka, A. Goto, W. G. Clark, P. Millet, J. Y. Henry, J. L. Gavilano, H. R. Ott, F. Mila, C. Berthier, M. Horvatic, Y. Tokunaga, P. Kuhns, A. P. Reyes, and W. G. Moulton, Phys. Rev. B **65**, 214413 (2002); cond-mat/0112203.

[45] Note that $U_{\text{eff}} \neq U_d$ and these two parameters have fairly different meaning. U_{eff} is the effective Coulomb repulsion in the mixed V $3d$ – O $2p$ band, while U_d is the repulsive potential applied to V $3d$ orbitals only.

[46] M. D. Johannes, J. Richter, S.-L. Drechsler, and H. Rosner, Phys. Rev. B **74**, 174435 (2006); cond-mat/0609430.

[47] The TB model included all the NN and NNN hoppings as well as a number of long-range hoppings. The largest transfer integral not listed in Table II is 10 meV. The respective J^{AFM} is about 1 K, i.e., well below the strongest interactions J_2 and J_3. Therefore, in the present discussion we neglect all the exchange couplings that do not run via PO_4 tetrahedra.

[48] The optimal value of U_d for estimating exchange couplings in $M(VO)_2(PO_4)_2$ (5 eV) is different from one for $Ag_2VOP_2O_7$ (6 eV, see Ref. 25). The difference is likely caused by the change of the basis sets in the computational program, see footnote 29.

[49] The value "$J_4 + J_5$" in Table III sums all the interactions between the atoms in positions (x, y, z) and $(\bar{x}, \bar{y}, z)$ or $(x + 1/4, \bar{y} + 1/4, z + 1/4)$ and $(\bar{x} + 1/4, y + 1/4, z + 1/4)$ of the $Fdd2$ space group. The TB model indicates two leading hoppings between these atoms: $t_6 = -9$ meV and $t_7 = -7$ meV. The hoppings provide an overall antiferromagnetic interaction of about 2 K that exceeds $J_4^{\text{AFM}} + J_5^{\text{AFM}}$. However, such an interaction is still considerably lower than the LSDA+U result.

[50] O. Janson, R. O. Kuzian, S.-L. Drechsler, and H. Rosner, Phys. Rev. B **76**, 115119 (2007).

[51] A. A. Tsirlin, R. Nath, C. Geibel, and H. Rosner, unpublished results on the magnetic properties of $NaVOPO_4$ and $Sr_2VO(PO_4)_2$. The crystal structures of these compounds include the chains of corner-sharing VO_6 octahedra similar to that in $M(VO)_2(PO_4)_2$. According to Sec. II, the V–O–V superexchange in the chain is impossible, since the half-filled d_{xy} orbital of vanadium is located in the plane perpendicular to the respective V–O bonds. Thus, the hopping should run via the PO_4 tetrahedron connecting two neighboring octahedra. The resulting transfer integral is very weak (~ 10 meV, similar to t_1 in Table II), therefore the ferromagnetic in-chain coupling dominates. Indeed, in $NaVOPO_4$ and $Sr_2VO(PO_4)_2$ we find ferromagnetic in-chain couplings of -3 K and -8 K, respectively.

[52] A. A. Tsirlin, A. A. Belik, R. V. Shpanchenko, E. V. Antipov, E. Takayama-Muromachi, and H. Rosner, Phys. Rev. B **77**, 092402 (2008); arXiv:0801.1434.

[53] S. Boudin, A. Guesdon, A. Leclaire, and M.-M. Borel, Int. J. Inorg. Mater. **2**, 561 (2000).